ELSEVIER

Materials Science and Engineering A246 (1998) 93–103

MATERIALS SCIENCE & ENGINEERING A

The dissolution of a stoichiometric second phase in ternary alloys: a numerical analysis

Fred Vermolen [a,b], Kees Vuik [b], Sybrand van der Zwaag [a,*]

[a] *Laboratory of Materials Science, Delft University of Technology, Rotterdamseweg 137, NL-2628 Al Delft, Netherlands*
[b] *Faculty of Technical Mathematics and Informatics, Delft University of Technology, Rotterdamseweg 137, NL-2628 Al Delft, Netherlands*

Received 11 July 1997; received in revised form 3 October 1997

Abstract

A general numerical model is described for the dissolution kinetics of stoichiometric second phases for one-dimensional cases in ternary systems. The model is applicable to both infinite and finite media and handles both complete and incomplete dissolution. It is shown that the dissolution kinetics of stoichiometric multicomponent second phase particles can differ strongly from that of the mono-element particles. The influence of the soft-impingement, ratio of the diffusion coefficients, stoichiometry, composition and the geometry of the dissolving stoichiometric phase is shown. The model is applied to an AlMgSi-alloy.

Keywords: Dissolution kinetics; Simulation; Alloys; Ternary alloys; Al alloys

1. Introduction

Heat treatment of metals is often necessary to optimise their mechanical properties both for further processing and for final use. During the heat treatment, the metallurgical state of the alloy changes. This change can either involve the phases being present or the morphology of the various phases. Whereas the equilibrium phases often can be predicted quite accurately from thermodynamic models, there are no general models for microstructural changes nor general models for the kinetics of these changes. In the latter cases both the initial morphology and the transformation mechanisms have to be specified explicitly. One of these processes, which is both of large industrial and scientific interest and amenable to modelling, is the dissolution of second phase particles in a matrix with a uniform initial composition.

To describe this particle dissolution in solid media, several physical models for binary alloys have been developed, incorporating the effects of long-distance diffusion [1–3] and non-equilibrium conditions at the interface [4–6]. These articles did not cover the technologically important dissolution of stoichiometric multicomponent particles in ternary alloys.

The phase transformations in steels for cases with a second alloying element has been studied in [7,8]. Reiso [9] has investigated the dissolution of Mg_2Si-particles in aluminium alloys mainly experimentally. He compared his results with a simple dissolution model based on analytical considerations holding for dissolving particles in infinite media. All analyses indicate that the addition of a second alloying element can influence the dissolution kinetics strongly.

However, none of these articles paid any attention to the effect of the particle geometry to the dissolution of particles in ternary alloys. The present article describes the dissolution of spherical and needle shaped particles, a planar medium and a segregration layer around a sphere. In many metallurgical situations, the thermal treatment also aims at the dissolution of the segregation layer around the grains. The latter two geometries may then be used to estimate the dissolution time of a segregration layer around a grain. In the mentioned articles no attention was drawn to the impact of all physical parameters on the overall dissolution kinetics.

* Corresponding author. Tel.: +31 15 2789111; fax: +31 15 27876730.

0921-5093/98/$19.00
PII S0921-5093(97)00734-X

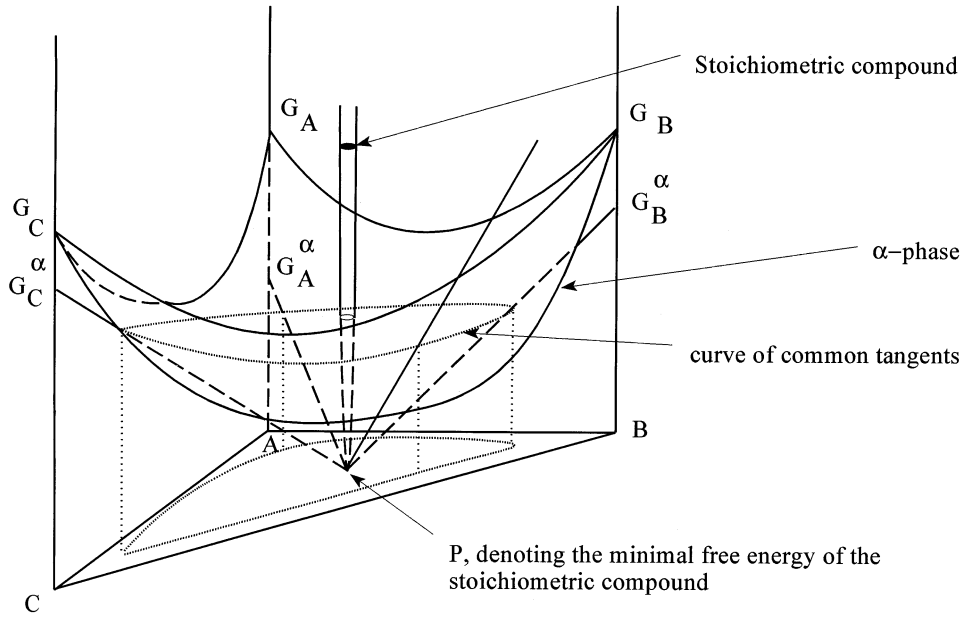

Fig. 1. A hypothetical Gibbs-free-energy surface in the Gibbs space.

2. Basic assumptions in the model

The model is based on the concept of local equilibrium, i.e. the interfacial concentrations are those as predicted by thermodynamics. The thermodynamics of the general case of a ternary alloy containing a single intermetallic compound is illustrated in Fig. 1. The Gibbs-free-energy of the matrix is indicated by the convex three-dimensional surface. The Gibbs-free-energy curve of the stoichiometric compound is needle shaped and has a very sharp minimum in point P (see Fig. 1). Equilibria between two phases are determined by an equal chemical potential in the phases, i.e. by a common gradient. Each plane including point P and tangent to the Gibbs surface of the α-phase can be described by:

$$G^{\alpha} = c_{\mathrm{A}} G^{\alpha}_{\mathrm{A}} + c_{\mathrm{B}} G^{\alpha}_{\mathrm{B}} + c_{\mathrm{C}} G^{\alpha}_{\mathrm{C}}, \tag{1}$$

where G^{α}_{k} represents the intersections of the planes with the k-axes ($k \in \{\mathrm{A}, \mathrm{B}, \mathrm{C}\}$). The requirement that all these planes include the stoichiometric phase, yields:

$$G^{\phi} = l G^{\alpha}_{\mathrm{A}} + m G^{\alpha}_{\mathrm{B}} + n G^{\alpha}_{\mathrm{C}}, \tag{2}$$

where l, m and n correspond to the stoichiometric phase $\mathrm{A}_l\mathrm{B}_m\mathrm{C}_n$ and G^{ϕ} corresponds to the Gibbs-free-energy of the stoichiometric compound, i.e. point P. As the values G^{α}_{k} are related to the Gibbs-free-energy of the pure component via the thermodynamic activity and for dilute solutions the laws of Henry and Raoult hold, hence the following hyperbolic relationship holds for a stoichiometric phase:

$$(c^{I}_{\mathrm{B}})^{m} (c^{I}_{\mathrm{C}})^{n} = K(T). \tag{3}$$

The isothermal intersections of a ternary phase diagram for two different temperatures have been sketched in Fig. 2, in which $T_1 < T_2$. If the alloy composition is such that its position is outside the regions α, β and γ, then the matrix composition can be obtained by the use of tie-lines. Increasing the temperature imposes a translation of the lines between subsequent phases further away from the corners of the triangle, which can imply that given a fixed composition, a different phase may become thermodynamically more favourable. If, after increasing the temperature such that the composition falls into one of the regions α, β or γ, then the second phase dissolves.

The ternary phase diagrams can predict quite accurately which phase and to what amount it will dissolve; they, however, can not predict the dissolution rate. An hypothetical case of an isothermal section of a ternary phase diagram is shown in Fig. 2.

For convenience, an alloy is considered with a composition near point A. Suppose that this composition falls into the three phase region $\alpha + \beta + \gamma$ for the initial temperature T_1 and suppose that the alloy is heated up to temperature T_2 such that the alloy composition falls into region α. Assuming diffusion to be the only rate-controlling process, then the interfacial concentrations have to be maximal. Therefore, the interfacial concentrations of both alloying elements then have to lie on curve k. Having two unknown interfacial concentrations to be determined, an additional constraint is needed for a unique determination of these concentrations. In many situations, the particles remain stoichiometric during dissolution [9], i.e. the translation of the interface due to both alloying elements is equal, resulting in:

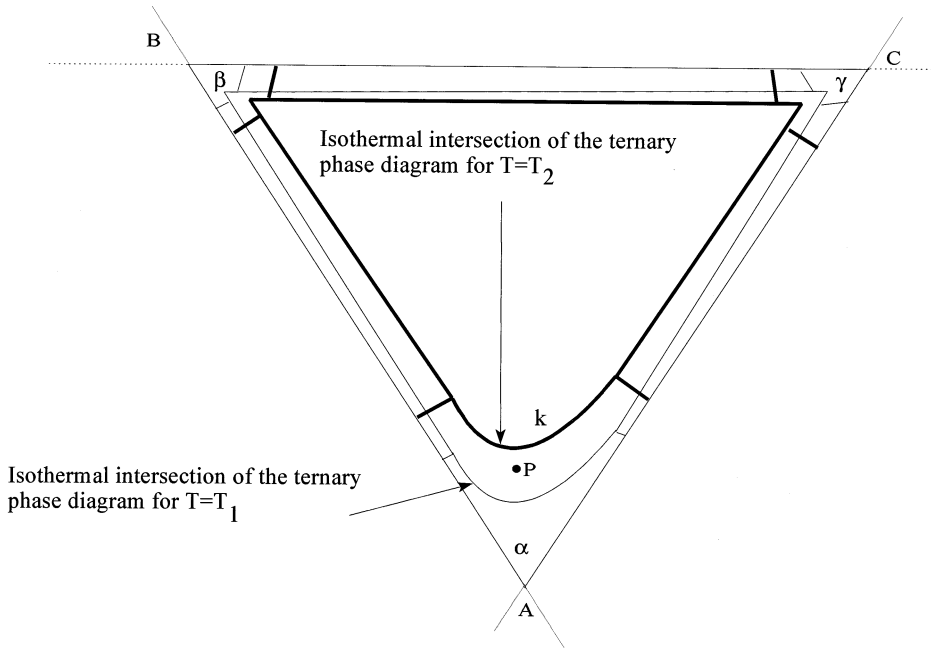

Fig. 2. An isothermal intersection of a hypothetical ternary phase diagram.

$$\frac{\mathrm{d}R(t)}{\mathrm{d}t} = \frac{D_{\mathrm{B}}}{c_{\mathrm{B}}^{\beta} - c_{\mathrm{B}}^{I}} [\underline{\nabla} c_{\mathrm{B}} \cdot \underline{n}]_{R(t)} = \frac{D_{\mathrm{C}}}{c_{\mathrm{C}}^{\beta} - c_{\mathrm{C}}^{I}} [\underline{\nabla} c_{\mathrm{C}} \cdot \underline{n}]_{R(t)}, \tag{4}$$

where c_{B}^{β} and c_{C}^{β} remain constant during the entire dissolution process, D_i represents the diffusion coefficient of the ith alloying element in the alloy, c_i^{β} represents the concentration of the ith element inside the particle and c_i^I is the interfacial concentration of the ith element ($i \in \{\mathrm{B}, \mathrm{C}\}$). Eq. (4) requires the knowledge of the concentration profile as to be obtained by the integration of Fick's Second Law for multicomponent diffusion. The basic formulation of Fick's Second Law describing multicomponent diffusion reads as [10,11]:

$$\frac{\partial c_i(\underline{r}, t)}{\partial t} = \underline{\nabla} \cdot \sum_{j=1}^{n-1} D_{ij} \underline{\nabla} c_j(\underline{r}, t), \tag{5}$$

where $c_i(\underline{r}, t)$ denotes the concentration of the ith element at position $\underline{r}$ and time t and D_{ij} represents the diffusion coefficients. The use of Eq. (4) combined with Eq. (3) yields sufficient boundary conditions at the interface.

For the most technologically interesting situations, the cross-diffusion coefficients D_{ij} are negligible compared with the 'diagonal' diffusion coefficients D_{ii}. Due to the lack of knowledge about the relationship between the diffusion coefficient and the matrix composition, the diffusion coefficient is taken to be independent of the matrix composition.

3. The numerical treatment

For each time step, the diffusion equation for both alloying elements has to be solved simultaneously. As a result of Eq. (4), the problem is non-linear. Therefore, an iterative method has to be used to solve this problem.

To provide a clear description of the iteration method, the description of the algorithm is split into a description of the solution method of the moving boundary problem and a subsequent description of the determination of the interfacial concentrations of both alloying elements.

3.1. The solution of the moving boundary problem

The numerical approach of the moving boundary problem for each diffusion equation has been carried out for a planar, cylindrical and spherical geometry and a spherical segregation layer around a spherical grain. For all these ideal geometries, the problem is reduced to a one-dimensional problem. Numerically these geometries only differ in the exponential factor of the position (which can be seen easily by a simple mass-balance).

When evaluating the interfacial position at each time step during the iteration process, a new initial boundary value problem is solved, in which the initial condition is given by the concentration that was evaluated at the last iteration. A finite difference method is applicable since the concentration profile in the matrix is continuous, at least up to the second derivative of position and the first derivative of time. The mesh is adjusted after each iteration such that the 0th mesh-surface coincides with the interfacial position. This has been done for the

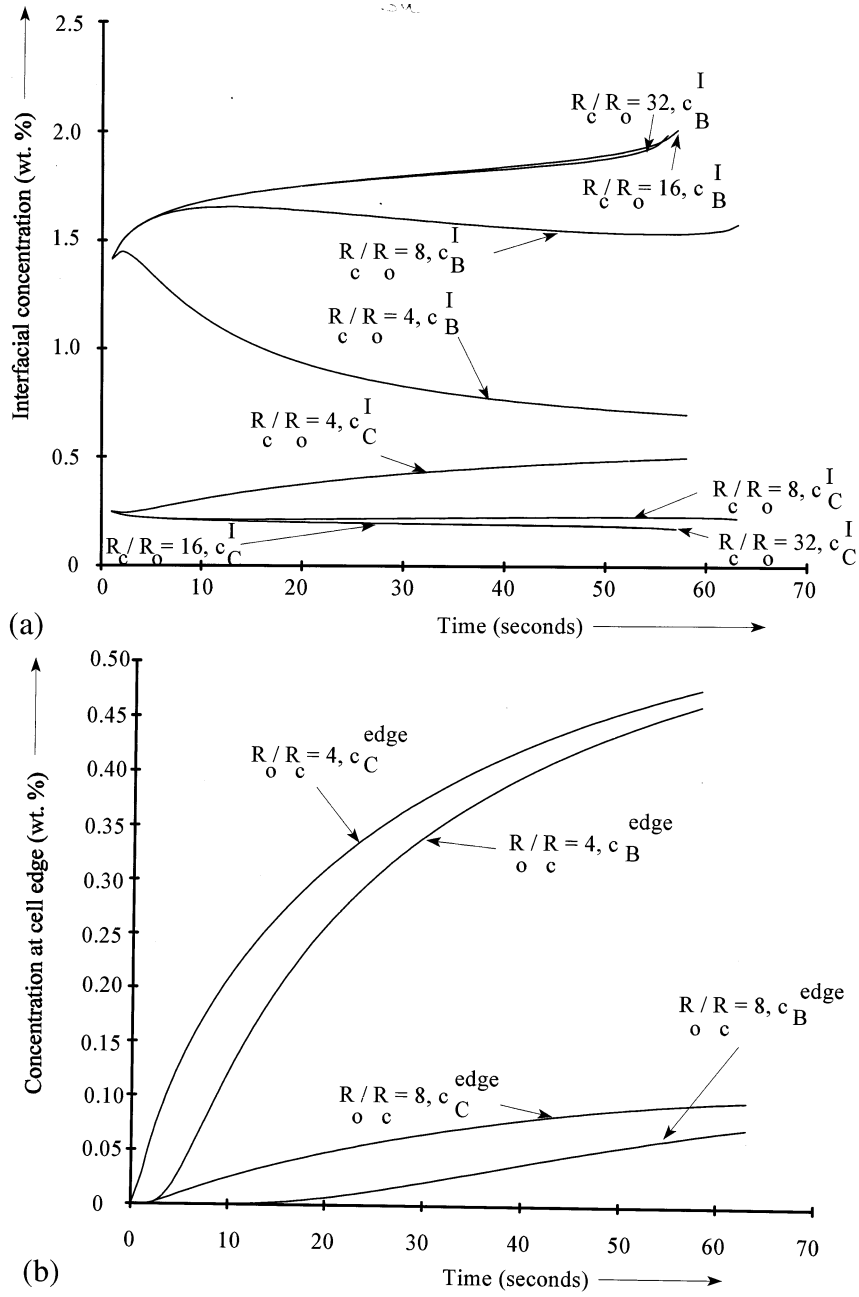

Fig. 3. The dissolution kinetics of a spherical stoichiometric particle for different R_c/R_0-ratios: The interfacial concentrations (a) and the concentrations at the cell edge (b) of both alloying elements and the particle radius (c) as a function of time.

following reasons: (1) the interface can be used as a mesh-surface, which can be used in the boundary condition at the interface and (2) the mesh is enlarged after each iteration. As the error smoothes out with iteration time and the absolute value of the concentration gradients decreases with iteration time, it is beneficial to have a coarser mesh which allows a higher computational speed.

The numerical procedure is also based on a mass-balance in each mesh-surface. This is to avoid the occurrence of singularities for curved surfaces as the particle size tends to zero or at the grain centre when describing the dissolution of a spherical segregation layer. For reasons of accuracy, a virtual gridpoint has been used behind the interfacial position and behind the cell edge or the grain centre. The introduction of the virtual gridpoints guarantees an overall accuracy of $O(dr^2)$, also at the boundaries. To avoid instability as much as possible, an implicit discretisation scheme has been chosen.

As the mesh is moving, the evaluation of the concentration profile can be summarised to proceed according to the following coarse algorithm:

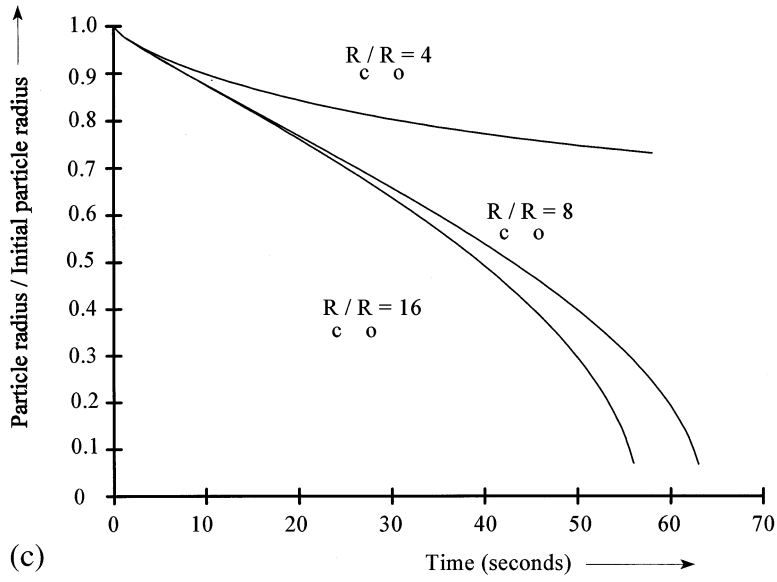

Fig. 3. (*Continued*)

1. The concentration profile at all mesh-surfaces is evaluated according to the diffusion equation using an implicit method from the former iteration.
2. The Stefan-condition at the interface is applied, causing a movement of the interface.
3. Distribution of the new mesh-surfaces, i.e. creation of the new mesh such that the 0th mesh-surface coincides with the moving boundary.
4. Determination of the concentration at the new mesh-surfaces by linear interpolation (a convective derivative yields the same results and is more suitable for two-/three-dimensional moving boundary problems).
5. Return to step 1, until the phase has dissolved.

Under the assumption that the diffusion coefficient is independent on the composition, Fick's Second Law, i.e. the diffusion equation for one-dimensional geometries, is generally given by:

$$\frac{\partial c_p(r,t)}{\partial t} = \frac{D_p}{r^a}\frac{\partial}{\partial r}\left\{ r^a \frac{\partial c_p(r,t)}{\partial r}\right\}$$
$$a \in \{0,1,2\},\ p \in \{\mathrm{B},\mathrm{C}\}, \tag{6}$$

where a is a geometric parameter, which equals 0, 1 and 2 for, respectively, planar, cylindrical and spherical geometries. In the remainder of this subsection the equations of the discretisation will be given, in these equations i refers to the mesh-surface and j refers to the time step. The subscript p, denoting the alloying element p, will be omitted in the remainder of this section. Moreover, the following definitions have been used:

$$\begin{aligned}
\Delta r_j &= \frac{R_c - R^j}{n}\\
r_i^j &= R_j + i\cdot\Delta r_j\\
r_i^{W,j} &= r_i^j - \frac{\Delta r_j}{2}\\
r_i^{E,j} &= r_i^j + \frac{\Delta r_j}{2}
\end{aligned} \tag{7}$$

Here R and R_c respectively, refer to the interfacial position and to the cell radius. Algebraically, the discretisation can be formulated as follows, for the bulk material:

$$\begin{aligned}
&\left\{\frac{1}{D\Delta t} + \frac{(r_i^{W,j+1})^a}{(r_i^{j+1})^a \Delta r_{j+1}^2} + \frac{(r_i^{E,j+1})^a}{(r_i^{j+1})^a \Delta r_{j+1}^2}\right\} c_i^{j+1}\\
&- \frac{(r_i^{W,j+1})^a}{(r_i^{j+1})^a \Delta r_{j+1}^2} c_{i-1}^{j+1} - \frac{(r_i^{E,j+1})^a}{(r_i^{j+1})^a \Delta r_{j+1}^2} c_{i+1}^{j+1}\\
&= \frac{1}{D\Delta t}\left\{ c_i^j + \frac{c_{i+1}^j - c_{i-1}^j}{2\Delta r_j}(r_i^{j+1} - r_i^j)\right\}
\end{aligned} \tag{8}$$

and at the interface:

$$\begin{aligned}
&- \frac{(r_0^{W,j+1})^a}{(r_0^{j+1})^a \Delta r_{j+1}^2} c_{-1}^{j+1} - \frac{(r_0^{E,j+1})^a}{(r_0^{j+1})^a \Delta r_{j+1}^2} c_1^{j+1}\\
&= \frac{1}{D\Delta t}\left\{ c_I^j + \frac{c_1^j - c_{-1}^j}{2\Delta r_j}(r_0^{j+1} - r_0^j)\right\}\\
&\quad - \left\{\frac{1}{D\Delta t} + \frac{(r_0^{W,j+1})^a}{(r_0^{j+1})^a \Delta r_{j+1}^2} + \frac{(r_0^{E,j+1})^a}{(r_0^{j+1})^a \Delta r_{j+1}^2}\right\} c_I^{j+1}
\end{aligned} \tag{9}$$

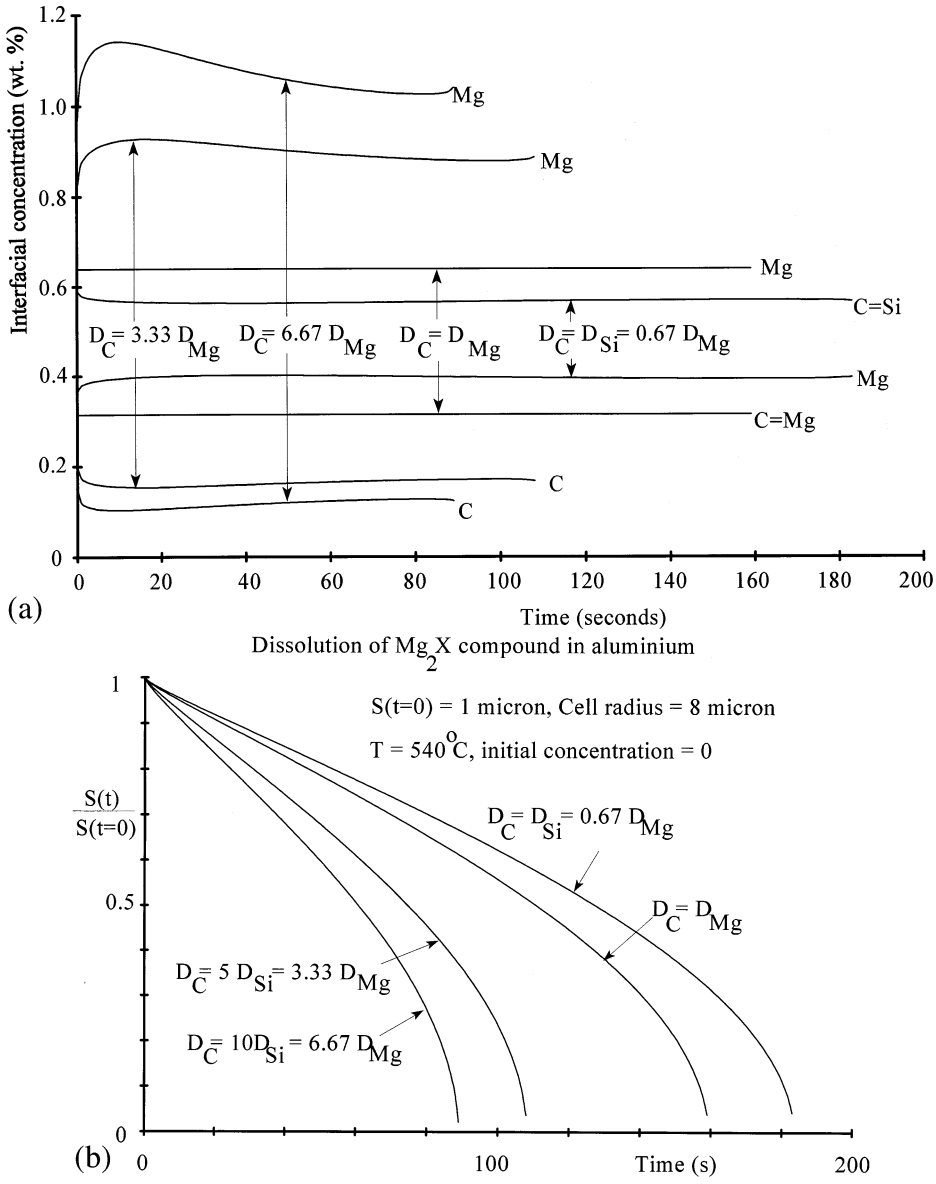

Fig. 4. The dissolution kinetics of a spherical stoichiometric particle for different D_2/D_1 ratios. The interfacial concentrations of both alloying elements (a), the particle radius (b) as a function of time.

The previous equation is not necessary for the computation of the concentration profile in the bulk material but it is used to determine the concentration gradient at the interface which is used to determine the interfacial velocity. In the vicinity of the interface we have:

$$\left\{\frac{1}{D\Delta t}+\frac{(r_1^{W,j+1})^a}{(r_1^{j+1})^a\Delta r_{j+1}^2}+\frac{(r_1^{E,j+1})^a}{(r_1^{j+1})^a\Delta r_{j+1}^2}\right\}c_1^{j+1}-\frac{(r_1^{E,j+1})^a}{(r_1^{j+1})^a\Delta r_{j+1}^2}c_2^{j+1}=\frac{(r_1^{W,j+1})^a}{(r_1^{j+1})^a\Delta r_{j+1}^2}c_I^{j+1}+\frac{1}{D_\Delta t}\left\{c_1^j+\frac{c_1^j-c_I^j}{\Delta r_j}(r_1^{j+1}-r_1^j)\right\} \quad (10)$$

and at the cell edge:

$$\left\{\frac{1}{D\Delta t}+\frac{(r_n^{W,j+1})^a}{(r_n^{j+1})^a\Delta r_{j+1}^2}+\frac{(r_n^{E,j+1})^a}{(r_n^{j+1})^a\Delta r_{j+1}^2}\right\}c_n^{j+1}-\left\{\frac{(r_n^{W,j+1})^a}{(r_n^{j+1})^a\Delta r_{j+1}^2}+\frac{(r_n^{E,j+1})^a}{(r_n^{j+1})^a\Delta r_{j+1}^2}\right\}c_{n-1}^{j+1}=\frac{c_n^j}{D\Delta t}. \quad (11)$$

Into Eqs. (9) and (10) the boundary conditions $c_0^j = c_I^j$ and $c_{n-1}^j = c_{n+1}^j$ have been substituted.

For the case of a layer of segregation around a spherical grain, the numbering is reversed and low numbers correspond to grid surfaces near the layer of segregation. The above equations are maintained except the following:

$$r_i^j = R_c - (R^j + i \cdot \Delta r_j)$$
$$r_i^{W,j} = r_i^j + \frac{\Delta r_j}{2} \quad . \tag{12}$$
$$r_i^{E,j} = r_i^j - \frac{\Delta r_j}{2}$$

The above system of linear equations that result from the finite difference discretisation can be arranged into a matrix equation, which can be solved using a three diagonal pivoting algorithm.

3.2. The determination of the interfacial concentrations

The solid solubilities of both alloying elements are linked by ternary phase diagrams, their relationship can considered as approximately hyperbolic, i.e. by Eq. (3). This must hold at the same time as Eq. (4). As the concentration profiles of both alloying elements depend on the interfacial concentrations, the concentration gradients of the elements also depend on the interfacial concentration. Hence, we are faced with the following non-linear problem:

$$f(c_B^I) = \frac{D_B}{D_C} \frac{c_C^\beta - c_C^I(c_B^I)}{c_B^\beta - c_B^I} \frac{[\underline{\nabla} c_B \cdot \underline{n}]_{R(t)}}{[\underline{\nabla} c_C \cdot \underline{n}]_{R(t)}} - 1 = 0. \tag{13}$$

From the combination of the initial boundary value problems and the relationship between both interfacial conditions for both elements it is clear that $\underline{\nabla} c_B \cdot \underline{n}$ and $\underline{\nabla} c_C \cdot \underline{n}$ also depend on the interfacial concentration c_B^I. $S(t)$ denotes the interfacial position at time t. So the problem has been reduced to obtaining a root for the above function f. No discontinuities, nor any singularities are to be expected for this function. Setting c_B^I very large minimises c_C^I, maximises $\underline{\nabla} c_B \cdot \underline{n}$ and sets $\underline{\nabla} c_C \cdot \underline{n}$ very negative, then $f > 0$, for the case of setting c_B^I such that $\underline{\nabla} c_B \cdot \underline{n}$ is sufficiently small, it follows that $f < 0$. For this continuous real function, it follows that at least one real root exists. To solve the above equation, a 'discrete Newton Raphson' iteration scheme is proposed and described in the remainder of this section.

The analytical approximate solution for the interfacial concentrations for the infinite planar medium in which a particle dissolves [9] can be used as the initial value for the iteration procedure at time $t = 0 + \mathrm{d}t$. For the subsequent times, the interfacial concentrations from the former iteration are used. These initial guesses that are put into the iteration process, guarantee a fast iteration process. As the function f can only be evaluated at discrete values of c_B^I, the function is evaluated at $c_B^I - \varepsilon$, c_B^I and $c_B^I + \varepsilon$, for $\varepsilon > 0$, obtaining the following iteration scheme, with an accuracy for the differentiation of f with respect to c_B^I of $O(\varepsilon^2)$:

Iterate:

$$c_B^I(p+1) = c_B^I(p) - \frac{2\varepsilon f(c_B^I(p))}{f(c_B^I(p) + \varepsilon) - f(c_B^I(p) - \varepsilon)}$$

In which the concentration profiles of both elements have to be evaluated at each iteration step, p, until $|c_B^I(p+1) - c_B^I(p)| < \varepsilon$, corresponding to $|f(c_B^I(p))| < \delta(\varepsilon) = |f(c_B^I(p) + \varepsilon) - f(c_B^I(p) - \varepsilon)|/2$.

ε Is a measure for the accuracy for c_B^I, the interfacial concentrations and $\delta(\varepsilon)$ is a measure for the deviation of f from zero, which depends on ε. From a numerical point of view, it is important to note that ε has to be sufficiently small but beyond the accuracy of the numerical scheme to evaluate the concentration. In most cases, the above iteration scheme converged within four iteration steps.

4. Results of computations

To observe the behaviour of the dissolution kinetics due to the addition of a second alloying element, a few sets of calculations have been carried out using the algorithm described in the previous section. In the first set of calculations, the influence of the ratio of the cell radius and the initial particle size on the dissolution kinetics has been investigated. The ratio D_C/D_B has been set equal to 10, in which the diffusion coefficient of the first element has been set equal to the diffusion coefficient of Si according to Fujikawa [12] for 803 K and the solubility product $K(T)$ has been set equal to 0.35. The initial matrix concentration has been set equal to zero for both elements and the stoichiometry has been set BC. The calculated results are shown in Fig. 3 for spherical geometry.

In Fig. 3(a) the interfacial concentrations of both elements have been plotted as a function of the dissolution time. From Fig. 3(a) it can be seen that the interfacial concentrations diverge from each other during the first stages of the dissolution process. In the calculations, diffusion has been assumed to be the rate determining step.

This means that the interfacial reactions, like the decomposition of the intermetallic compound in the particle, are assumed to proceed infinitely fast for both elements. To maintain the stoichiometry of the particle, the number of atoms of both elements leaving the particle are uniquely coupled. For the case in Fig. 3, in which the weight percentages of both elements are equal, the number of atoms leaving the particle is similar for both elements. The atoms of the faster element move away very fast from the particle, while the sluggish atoms move slowly away from the particle. Due to the slow atomic movement of the sluggish element, the slower atoms accumulate at the interface as the interfacial area decreases, whereas the faster

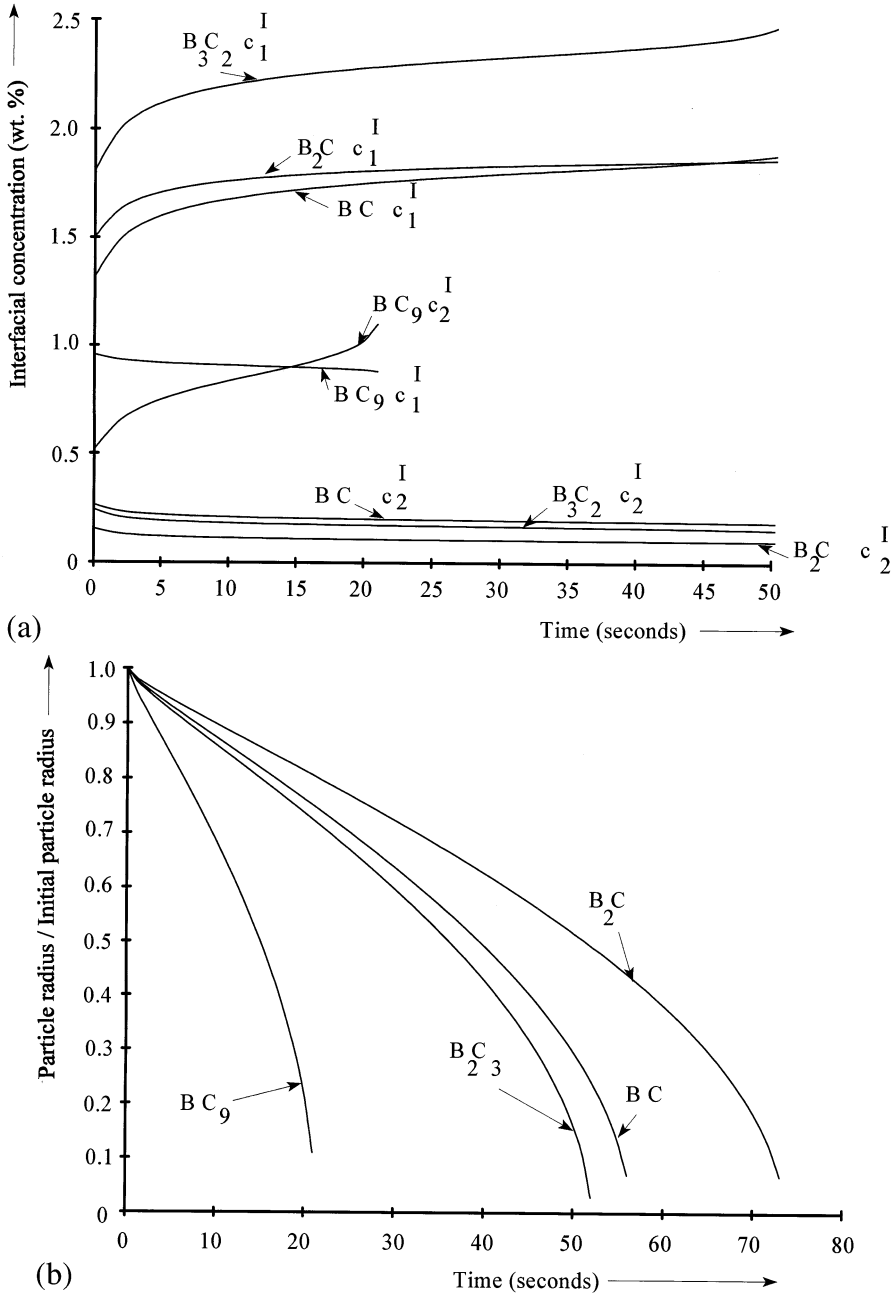

Fig. 5. The dissolution kinetics of a spherical stoichiometric particle for different stoichiometries. The interfacial concentrations of both alloying elements (a) and the particle radius (b) as a function of time.

atoms move rapidly deeper into the matrix. This causes the diverging behaviour between both interfacial concentrations in the early stages of the dissolution process.

As dissolution proceeds, the faster atoms accumulate at the cell edge, the concentration gradients at the interface of both alloying elements decrease. As the interfacial reactions are assumed to proceed infinitely fast and the diffusion rate is lowered due to the accumulation of the alloying atoms at the cell edge, especially of the faster atoms now, an accumulation of the faster atoms at the interface results. Thereby and due to the maintainance of the particle stoichiometry, the interfacial concentrations converge towards each other. This effect becomes more pronounced for smaller R_c/R_0 ratios. Fig. 3(b) displays the normalised particle radius as a function of time for different R_c/R_0 ratios. This, in combination with the accumulation of the sluggish atoms at the interface during the early stages of the dissolution process, causes the global extrema for the interfacial concentrations for both alloying elements.

For a further investigation of the occurrence of the influence from the addition of a second element, a set of calculations has been carried out for the case that

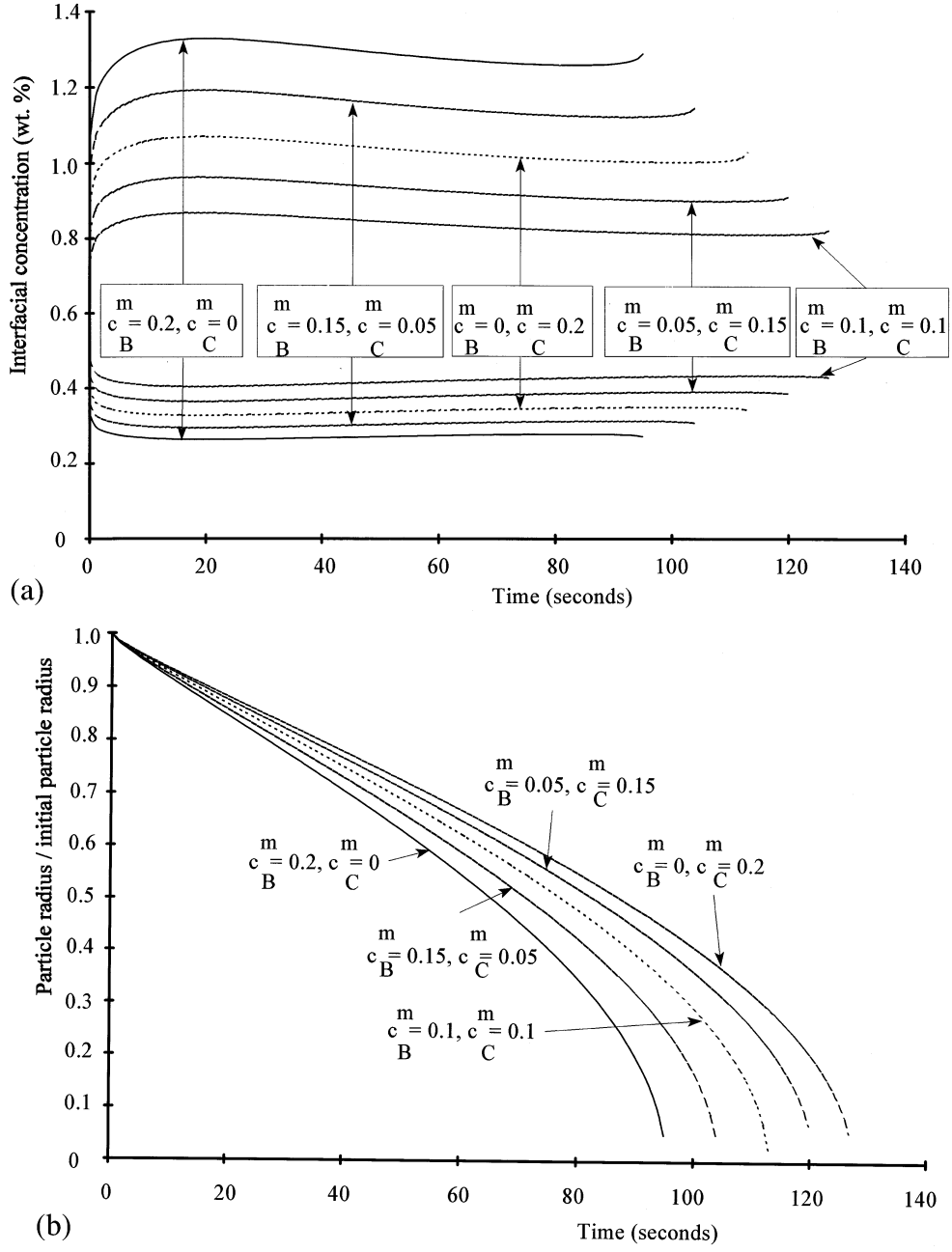

Fig. 6. The dissolution kinetics of a spherical particle for different initial matrix compositions. The interfacial concentrations of both alloying elements (a) and the particle radius (b) as a function of time.

$R_c/R_0 = 8$ and for different values of D_C/D_B. The dissolution kinetics for the case of a AlMg-based alloy are shown in Fig. 4. For this case B = Mg, i.e. $D_B = D_{Mg}$, and C is the additional alloying element.

Again the particle stoichiometry was BC and the initial matrix concentrations was for both elements 0. The solubility product was again 0.35. Curve I corresponds to the case that the second element is Si. The diffusion coefficient of Si is ≈ 0.67-times the diffusion coefficient of Mg. For the diffusion coefficient of Mg, the diffusion coefficient of Yamane [13], corresponding to 803 K, has been used. Curve II corresponds to the case that the diffusion coefficient of the second alloying element equals the diffusion coefficient of Mg, i.e. this case corresponds to a binary alloy. Curves III and IV, respectively, correspond to the cases that the diffusion of the second element equals 5- and 10-times the diffusion coefficient of Mg. It is observed that the dissolution times do not depend linearly on the diffusion coefficient of the second element.

Due to the addition of a second faster element, the interfacial concentration of the sluggish element is rather large (see Fig. 4(a)), causing a larger absolute value of its concentration gradient. This causes a higher

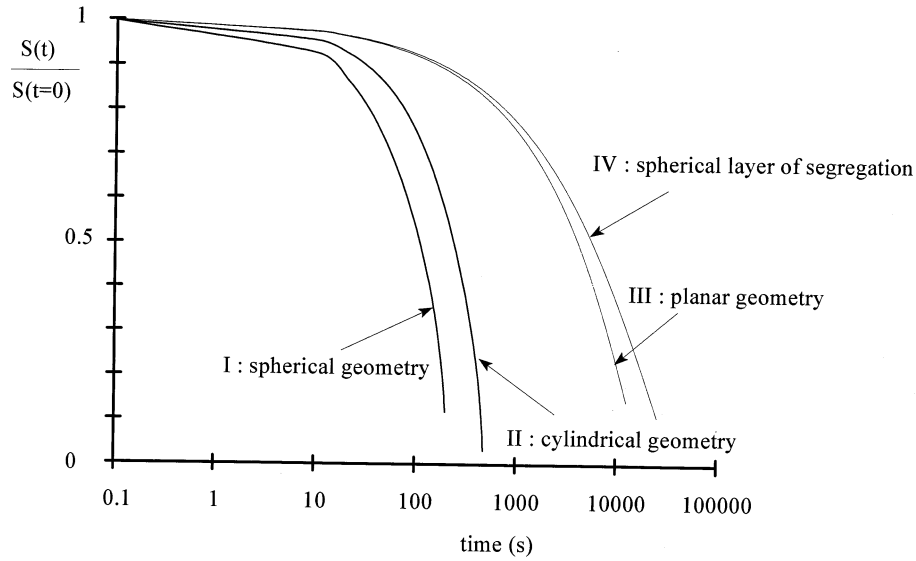

Fig. 7. The dissolution kinetics of different geometries of stoichiometric Mg_2Si phase for a temperature of 803 K. The initial size is 1 μm and the overall composition is 0.34 mass% Si and 0.54 mass% Mg.

effective driving force for the dissolution of the sluggish element and thus an enhancement of the dissolution kinetics. Thereby, the dissolution kinetics are enhanced by the addition of a faster element (see Fig. 4(b)).

The next numerical experiment considers the influence of the stoichoimetry of the dissolving particle. It has been assumed here that the solubility product does not change with stoichoimetry, i.e. the Gibbs-free-energies of the pure alloying elements are equal. The results have been plotted in Fig. 5.

All curves correspond to the same ratio of the diffusion coefficients: $D_C/D_B = 10$. The stoichoimetries have been varied such that $c_B^\beta = 10$, 35 and 50 wt.%. The calculations have been done for the spherical geometry with initial particle radius of 1 μm and a cell radius 10 μm. The solubility product was 0.35 and the initial matrix concentrations of both elements was set at zero. The interfacial concentrations of both elements have been plotted as a function of time in Fig. 5(a). For this cell size, the concentrations at the cell size have not changed very much. Therefore, the diverging behaviour of the interfacial concentrations can be observed exept for the case of $c_B^\beta = 10$, here the curves even intersect. From the theory of Reiso for the dissolution of a binary precipitate in an infinite medium ([9]: page 523), two approximate limits can be deduced for the ratio of the interfacial concentrations of both elements:

Table 1
The cell sizes for the different geometries

Curve	I	II	III	IV
Cell size (μm)	5	11.5	125	373

$$\sqrt{\frac{D_C}{D_B}}\frac{c_B^\beta}{c_C^\beta} < \frac{c_B^I}{c_C^I} < \frac{D_C}{D_B}\frac{c_B^\beta}{c_C^\beta}. \tag{14}$$

The lower and higher limit, respectively, correspond to the initial and final stages of the dissolution process. From this it follows that the ratio of the interfacial concentrations for the case that the ratio of diffusion coefficients $D_C/D_B = 10$ and the stoichiometry of 1/9 (here the concentration of the faster element in the particle is largest), that here the limits for the ratio of the interfacial concentrations are given by approximately 0.35 and 1.11, explaning that an intersection behaviour of the corresponding curves. For this case it can also be observed that the interfacial concentration of the fast element now starts beyond the interfacial concentration of the slow element. This may be explained as follows: due to a much larger amount of fast atoms leaving the particle to maintain the particle stoichiometry. In the later stages of the dissolution process, the atoms at the interface of the faster atoms diffuse into the matrix very rapidly, causing a decrease of the interfacial concentration of the faster element. As the slower atoms are accumulated at the interface, their interfacial concentration therefore increases. For stoichiometries with either, relatively, many A or B atoms, the dissolution kinetics approach the dissolution kinetics of a unary precipitate.

Fig. 6 considers the influence of the initial matrix composition on the dissolution kinetics. The calculations have been carried out for $R_c/R_0 = 8$ ($R_0 = 1$ μm) and $D_C/D_B = 5$. The solubility product, $K(T)$, was set at 0.35. The matrix composition has been varied such that all curves correspond to the same total amount of alloying elements. Thereby, the stoichiometry in the matrix varies and the overall composition of alloying

elements in the alloy is either stoichiometric or non-stoichiometric. At the very early stages of the dissolution process, we have:

$$\frac{\mathrm{d}R(t)}{\mathrm{d}t}=\frac{c_{\mathrm{B}}^{I}-c_{\mathrm{B}}^{m}}{c_{\mathrm{B}}^{\beta}-c_{\mathrm{B}}^{I}}\sqrt{\frac{D_{\mathrm{B}}}{\pi t}}=\frac{c_{\mathrm{C}}^{I}-c_{\mathrm{C}}^{m}}{c_{\mathrm{C}}^{\beta}-c_{\mathrm{C}}^{I}}\sqrt{\frac{D_{\mathrm{C}}}{\pi t}} \tag{15}$$

and of coarse between the interfacial concentrations, the hyperbolic relationship holds (viz. Eq. (3)). For these cases, that the total amount of alloying elements is similar, it can be proven that the derivatives of both $(c_{\mathrm{B}}^{I}(c_{\mathrm{B}}^{m})-c_{\mathrm{B}}^{m})$ and c_{B}^{I} with respect to c_{B}^{m} are positive. As $c_{\mathrm{B}}^{\beta}\gg c_{\mathrm{B}}^{I}$, it can be seen from the last equation that the dissolution kinetics will be more rapid for a larger amount of sluggish alloying element in the total composition, as long as the particle remains stoichiometric.

5. Application to an AlSiMg-alloy

The described algorithm has been applied to the dissolution of a stoichiometric Mg_2Si-phase. In commercial alloys, this phase may have different geometries. The phase can either be present in the grain, except in the precipitate free zone near the grain boundary, or at the grain boundary. The dissolution kinetics of the Mg_2Si-phase at the grain boundary can be approximated one-dimensionally either by a spherical segregation layer around a grain or by an infinite plate of finite thickness. Both approaches provide a higher and lower limit of the dissolution time.

The Mg_2Si-phase may also be present in the form of needles. For this case to be one-dimensional, the dissolution kinetics of the needles have been approximated by an infinitely long cylinder. Here it has been assumed that dissolution proceeds radially. However, due to surface tension effects, especially at the very sharp angle of the cylinder, the decrease of the cylinder length of the Mg_2Si-phase might be important as well.

For the cases that an AlMgSi-alloy has been cooled very slowly, the precipitates may be large and have a rounded geometry. A comparison in the dissolution kinetics for all these one-dimensional geometries has been given in Fig. 7.

All curves correspond to the same initial size of the dissolving stoichiometric Mg_2Si-phase of 1 μm, dissolution temperature of 803 K and same composition (0.34 mass% Si and 0.54 mass% Mg) and solubility product, $K(T)=0.35$. The values of the cell sizes are given in Table 1. The initial matrix concentrations of Si and Mg have, respectively, been set equal to 0.06 and 0.025 mass%.

For the cases of a spherical and cylindrical shape of the Mg_2Si-phase, the dissolution kinetics are enhanced by the decrease of the free surface. However, for the case of a spherical segregation layer, the dissolution kinetics are delayed as a result of an increase of the free surface and the increasing difficulty for the alloying elements to diffuse deeper into the aluminium matrix.

6. Conclusions

A model has been developed suitably for the dissolution of a stoichiometric phase in a ternary alloy. It is shown quantitatively that the dissolution kinetics of a stoichiometric phase in a ternary alloy is determined by physical parameters (the diffusion coefficient of both alloying elements, solid solubities, particle composition and stoichiometry), compositional parameters (the ratio of the cell size and the initial particle radius, initial matrix concentrations of both element) and particle geometry (spherical, cylindrical, planar or a spherical layer of segregation).

References

[1] M.J. Whelan, Met. Sci. J. 3 (1969) 95.
[2] U.L. Baty, R.A. Tanzilli, R.W. Heckel, Met. Trans. 1 (1970) 1651.
[3] U.H. Tundal, N. Ryum, Met. Trans. 23A (1992) 433.
[4] F.V. Nolfi Jr., P.G. Shewmon, J.S. Foster, Trans. Met. Soc. AIME 245 (1969) 1427.
[5] H.B. Aaron, G.R. Kotler, Met. Trans. 2 (1971) 393.
[6] F.J. Vermolen, S. Van der Zwaag, Mater. Sci. Eng. A220 (1996) 140.
[7] J. Ågren, J. Phys. Chem. 43 (1981) 421.
[8] J.M. Vitek, S.A. Vitek, S.A. David, Metall. Mater. Trans. 26A (1995) 2007.
[9] O. Reiso, N. Ryum, J. Strid, Met. Trans. 24A (1993) 2629.
[10] L. Onsager, Phys. Rev. 37 (1931) 405.
[11] J.S. Kirkaldy, D.J. Young, Diffusion in the Condensed State, The Institute of Metals, London, 1987.
[12] S. Fujikawa, K. Hirano, Y. Fujikawa, Met. Trans. 9A (1978) 1811.
[13] M. Yamane, J. Mater. Sci. 18 (1983) 2679.